



Full Length Article

Comparison of bulk basic properties with different existing Ni-Fe-O empirical potentials for Fe_3O_4 and NiFe_2O_4 spinel ferrites

Óscar A. Restrepo^{a,b,*}, Óscar Arnache^c, J. Restrepo^a, Charlotte S. Becquart^d, Normand Mousseau^e

^a Grupo de Magnetismo y Simulación G+, Instituto de Física, Universidad de Antioquia, A.A. 1226, Medellín, Colombia

^b Grupo de Biofísica, Instituto de Física, Universidad de Antioquia, A.A. 1226, Medellín, Colombia

^c Grupo de Estado Sólido-GES, Universidad de Antioquia, A.A. 1226, Instituto de Física, Medellín, Colombia

^d Univ. Lille, CNRS, INRAE, Centrale Lille, UMR 8207 - UMET - Unité Matériaux et Transformations, F-59000 Lille, France

^e Département de physique et Regroupement québécois sur les matériaux de pointe, Université de Montréal, Case postale 6128, succursale centre-ville, Montréal, QC H3C 3J7, Canada



ARTICLE INFO

Keywords:

Molecular dynamics
Bulk properties spinel ferrites
Elastic constants
MEAM
Buckingham potential
Morse-Buckingham potential
Elastic constants NiFe_2O_4 Fe_3O_4
Spinel vacancy

ABSTRACT

Accurate empirical potentials for the simulation of magnetite Fe_3O_4 and nickel-ferrite NiFe_2O_4 spinel systems are of fundamental importance for understanding their structural stability. To better understand how existing empirical potentials for Ni-Fe-O systems describe the spinel physics, we perform comparisons of some of the most important bulk properties. Elastic constants, lattice parameters, energies and Debye temperatures are computed and compared with previously published data of density functional theory (DFT) and experiments found in the literature. We find that all the potentials predict the spinel geometry well whereas there are discrepancies in bulk properties. The MEAM becomes unstable at high temperature for NiFe_2O_4 , although it gives the best prediction of static properties at zero temperature whereas under induced pressure or high temperature, Buckingham types offer more stability. In general, for static properties and if computational speed is required—and in the case of Fe_3O_4 no distinction between normal or inverse is demanded—MEAM should be preferable. However, if dynamics at some temperature and specific ordering are important, Buckingham types, although more computationally expensive, should be used.

1. Introduction

The study of spinel ferrites is important from a physical and chemical point of view [1]. Beyond their fundamental importance, they are used for several technological applications in catalysis, corrosion, adhesion at metal-oxide interfaces in composite materials, materials for preventing impurity adhesion, and identifying possible roles in spintronic devices and other new technologies, etc. [2]. Among those, spinel ferrites such as trevorite—also known as nickel-ferrite NiFe_2O_4 (henceforth NFO)—and magnetite Fe_3O_4 (henceforth FO) are of special interest because of their magnetic and electrical properties and possible applications to spintronics [3,4], among others. In terms of current applications, magnetite is one of the most important ferrimagnetic materials for industrial applications such as data storage, while trevorite have possible applications in the fabrication of antennas and batteries [5,6,7,8,9]. Beyond those, spinel structures have potential applications in

permanent magnets, microwave absorbers, chemical sensors, biomedicine, etc. [10,11].

Both NFO and FO present a spinel structure of the form AB_2O_4 (Fd $\bar{3}m$, no. 227) [12], with a unitary cell that counts 56 ions, where O ions fill 32 anions O-sites while cations (Ni or Fe) fill 8 tetrahedral A-sites and 16 octahedral B-sites. In normal spinels, A-sites are filled with A-ions and B-sites with B-ions whereas inverse spinels represent structures where A-sites are filled with B-ions and B-sites are filled randomly with A-ions and B-ions. Experimentally, the Mössbauer spectroscopy is one of the most reliable methods to determine the iron cation and anion distribution. High resolution X-ray diffraction can also determine the distribution as well as the geometry of spinels using the Rietveld refinement [13].

Due to the large unit cell and long-range interactions, the theoretical characterization of these materials, including defect diffusion, extended defects, migration and surface energies, and more, requires handling

Abbreviations: NFO, NiFe_2O_4 ; FO, Fe_3O_4 .

* Corresponding author.

<https://doi.org/10.1016/j.commsci.2022.111653>

Received 1 February 2022; Received in revised form 26 June 2022; Accepted 8 July 2022

Available online 19 July 2022

0927-0256/© 2022 Published by Elsevier B.V.

Table 1

Potentials found for Ni-Fe-O systems and tested with spinel ferrites NFO and FO. There are three versions of 1NN-MEAM: Ohira's papers [2,18] use, $\rho = \frac{2}{\rho_0(1+e^{-r})}$, alternatively Baskes [39] proposes $\rho = \rho_0\sqrt{1+\Gamma}$, which is tested here with Ni or Fe or both; O always uses $\rho = \rho_0\frac{2}{1+e^{-r}}$ (for details see Section 2 below).

Spinel ferrite NFO	Magnetite FO
1. Buckingham (Buck-1 params) [14].	1. Buckingham (Buck-3 params) [17].
2. Buckingham (Buck-2 params) [15,16].	2. 1NN-MEAM-1 (For Fe, $\rho = \rho_0\frac{2}{1+e^{-r}}$) [2].
3. Buckingham-Morse (Buck-Morse params) [17].	3. 1NN-MEAM-2 (For Fe, $\rho = \rho_0\sqrt{1+\Gamma}$) [2,39].
4. 1NN-MEAM-1 (For all $\rho = \rho_0\frac{2}{1+e^{-r}}$) [2,18].	4. EAM-SM (Embedded atom method Streitz-Mintmire). Unstable under minimization [19].
5. 1NN-MEAM-2 (For Ni, $\rho = \rho_0\sqrt{1+\Gamma}$) [2,39].	5. Tersoff (Unstable with magnetite, useful for other allotropes) [24].
6. 1NN-MEAM-3 (For, Ni, Fe, $\rho = \rho_0\sqrt{1+\Gamma}$) [2,39].	6. Shell model [26]. (Not used here).
7. EAM-SM (Embedded atom method Streitz-Mintmire). Unstable under minimization [19].	7. 2NN-MEAM with Ohira's parameters for Fe-O (no good spinel bulk properties) [21,2].
8. 2NN-MEAM with Ohira's parameters for Fe-O, Ni-O (no good spinel bulk properties) [21,2].	8. EAM + Charge Equilibration (not used here) [72]

systems counting many hundreds to many thousands of atoms and more, which make them unsuitable for *ab initio* approaches. It is therefore necessary to turn to empirical potentials, which must be able to describe accurately the physics involved. A review of the literature reveals only a handful of potentials that could be suitable for molecular dynamics (MD) or kinetic Monte Carlo (KMC) simulations. Yet, no comparison regarding the range of applicability of these potentials is available, which limits progress in this field.

For trevorite NFO we consider the following potentials: Buckingham with two parameterizations [14,15,16], Buckingham-Morse [17] and the modified embedded atom method potential with first nearest-neighbors interactions (1NN-MEAM) parametrized by Ohira [2]. We also test two density functions proposed by Baskes [18]. There are other potentials for Ni-Fe-O systems but these are not appropriate for NFO or FO spinels. For instance, the charge transfer ionic-embedded atom method potential for the O-Al-Ni-Co-Fe [19] has been tried, but is not considered here as we find that it does not predict stable spinels. Also, Lee's web [20] page offers some parameterizations with the 2NN-MEAM formalism where 2NN means including second nearest-neighbors interactions and the corresponding bibliography for pure systems like Ni, Fe, O and mixed Fe-Ni [21]. However, parameters for Ni-O and Fe-O bonds are not given and using Ohira's parameters for these

Table 2

Buckingham spinel parameters for NiFe₂O₄ (Buck-1, Buck-2) and Fe₃O₄ (Buck-2) systems.

Pair	z_i	z_j	A_{ij} (eV)	ρ_{ij} (Å)	C_{ij} (eVÅ ⁶)	B_{ij} (eVÅ ²⁴)	D_{ij} (eV/Å ²)	n	r_0 (Å)
NFO, Buck-1 [14]. Ions adopt partial charges.									
O—O	-1.2	-1.2	2029.2204	0.343645	192.58	46.462	-0.32605	3.430	1.9376
NiO	+1.2	-1.2	12987.7832	0.203164	35.994	73.158	-14.550	3.024	1.0274
FeO	+1.8	-1.2	11777.0703	0.207132	21.642	104.203	-32.110	2.670	0.9302
FeFe, NiNi, NiFe (only Coulomb term used)									
NFO, Buck-2 ([15,16]). Ions adopt nominal charges.									
O—O [16]	-2	-2	9547.96	0.2192	32				
NiO [15]	+2	-2	775.0	0.3250	0				
FeO [16]	+3	-2	1414.6	0.3128	0				
FeFe, NiNi, NiFe (only Coulomb term used)									
FO, Buck-3 [16]. Ions adopt nominal charges.									
Fe ³⁺ O ²⁻	+3	-2	1414.6	0.3128	0				
Fe ²⁺ O ²⁻	+2	-2	649.1	0.3399	0				
O ²⁻ O ²⁻	-2	-2	9547.96	0.2192	32				
FeFe, NiNi, NiFe (only Coulomb term used)									

binaries, we do not recover the correct structure after minimization, even though MEAM is designed to fit to experimental parameters for mixed types Fe-Ni, Fe-O and Ni-O. In recent papers [22,23], Lee's group proposed an interesting formalism where they combine 2NN-MEAM with a charge equilibration (Qeq) concept to overcome short range problems in ionic systems, but they do not have parameterizations for Ni-O or Fe-O interactions yet.

In the case of magnetite FO, we assess 1NN-MEAM and Buckingham potentials. We have also found a Fe-O Tersoff potential [24], however it does not properly describe magnetite, but it works well for other allotropes. There is also found an embedded atom method (EAM) potential combined with the charge equilibration method [72], which allows more realistic simulations as charges are not fixed, although this model is not used here. The mechanical properties of FO and other Fe-oxides can be also studied using the GULP package [25] with a shell model potential [26]. However, if only core-core interactions are considered, it resumes to Buckingham types used here.

The main goal of this work is to compare these different empirical potentials as they are applied to trevorite NFO spinel and magnetite FO spinel systems. More specifically, we assess whether these short-range and long-range potentials are able to describe the main structural properties of the spinel systems NFO and FO. To do so, we compare the various potentials to density functional theory (DFT), experimental results reported in the literature and between themselves.

Our simulations are performed using the Large-scale Atomic/Molecular Massively Parallel Simulator (LAMMPS) [27]. In this paper, we focus on the lattice constant a , the anion parameter u , the elastic constants and their derived quantities: bulk modulus B , Poisson ratio ν , rigidity modulus (or shear modulus) G , Young modulus E and the Zener anisotropic factor A ; all at zero temperature. We also evaluate the vacancy formation energy as vacancies are one of the most important type of defects in solid materials [28]. Finally, we check spinel stability for temperature ranging from 100 K to 2000 K. Comparing results for these various properties allows us to make recommendations as to which potential, if any, is most appropriate for specific research questions.

2. The implemented empirical potentials

A list of the potentials found for Ni-Fe-O systems is summarized in Table 1. Below, the description of the potentials implemented here with spinel ferrites NFO and FO.

2.1. Buckingham types

The simplest way to describe a spinel is by using a combination of a Coulomb pair potential and Buckingham empirical potentials. The anion-anion and anion-cation interactions can be handled by

Table 3

Buck-Morse parameters for NFO [17], the charges are +1.2 for Ni, +1.8 for Fe, and -1.2 for O.

	A (eV)	$\rho(\text{Å})$	C (eVÅ ⁶)	D (eV)	β (Å ⁻¹)	r^* (Å)
O—O	560.93434	0.360000	4.20	—	—	—
O—Ni	284.09782	0.362661	—	2.4196868	2.00	1.80
O—Fe	118.05851	0.416163	—	1.3120262	2.00	1.80
(Ni, Fe)— (Ni, Fe)	113.63134	0.482105	—	—	—	—

$$U_{ij} = \frac{z_i z_j e^2}{4\pi\epsilon_0 r_{ij}} + A_{ij} \exp\left(\frac{-r_{ij}}{\rho_{ij}}\right) - \frac{C_{ij}}{r_{ij}^6} + D_{ij} \left[\exp\left(-2\beta_{ij}(r_{ij} - r_{ij}^*)\right) - 2\exp\left(-\beta_{ij}(r_{ij} - r_{ij}^*)\right) \right] \quad (3)$$

Parameters (Buck-Morse) are shown in Table 3. This potential was originally used to simulate NiCr₂O₄ and FeCr₂O₄ spinels, however as it is fitted from the respective binary systems, here we test it for a NiFe₂O₄ spinel. To ensure neutrality for Fe we use a charge of +1.8 instead of the +1.2 reported in Ref [17]. We assume that this is correct because Buckingham plus Morse terms give the short-range cohesion energy of non-ionized atoms whereas the Coulomb term corresponds to the ionization (how much charge is removed from a neutral atom). The same approximation is applied by Oliver et al. Ref [15] for interactions of Ni^{2+/3+}-O²⁻, in nickel oxides. This potential fails at short distances $\lesssim 1$ Å, but is suitable for problems involving stable structures and energy minimizations.

2.3. Modified embedded atom method (MEAM)

The MEAM potential [30,31] is a variation of the embedded atom method (EAM) [32], which includes angular dependent interactions implemented via the electron density term. There are several formalisms. The original version of MEAM was proposed by Baskes [33] and is now known as 1NN-MEAM. There is a second one called second-nearest neighbor modified embedded-atom method (2NN-MEAM) developed by Lee and collaborators [34,35]. Although the functional form of the MEAM potential remains the same, through the years several specific functions have been proposed. For example, some have introduced additional terms to describe the electronic density [36] and reproduce the universal equation of state—the Rose form [37]—which is used in the reference structure construction [33,34,35]. The Rose form is

$$E^u(R) = -E_c(1 + a^* + da^{*3})e^{-a^*}, \quad (4)$$

$$a^* = \alpha\left(\frac{R}{r_e} - 1\right), \quad (5)$$

where R is the distance between the interacting atoms in the reference structure. The parameters E_c , r_e , B , and Ω are the cohesive energy (or sublimation energy), the equilibrium distance used to fit the properties of each atom, the bulk modulus and the atomic volume, at the reference structure, respectively; d is a variable parameter, which for older bibliography is set to zero (for example the first papers of Baskes [33,34] or even some recent papers[38]). The parameter α is known as the exponential decay factor for the universal energy function. Some reports do not give α but rather provide the bulk modulus B , as they are related by

$$\alpha = \sqrt{\frac{9B\Omega}{E_c}}. \quad (6)$$

Generally, all these parameters can be obtained from experiments or DFT. In the case of spinel systems, only few papers have been found with this potential. Specifically, we consider the 1NN-MEAM versions of Ohira et al. [2,18] for NFO and FO spinel systems. The background electron density implemented in Ohira's parameterization, labelled as MEAM-1 is

$$\rho = \rho_0 \frac{2}{1 + e^{-\Gamma}}, \quad (7)$$

where ρ_0 is a scaling factor and the ratios between atomic electron densities of the constituent elements are required (for pure systems they can be set to one) [33,34], Γ , is the effect of the angular terms given by

$$U_{ij}(r) = \frac{z_i z_j e^2}{4\pi\epsilon_0 r_{ij}} + A_{ij} \exp\left(\frac{-r_{ij}}{\rho_{ij}}\right) - \frac{C_{ij}}{r_{ij}^6}, \quad (1)$$

where $1/4\pi\epsilon_0 = 9 \times 10^9 \text{N}\cdot\text{m}^2\cdot\text{C}^{-2} = 14.399645 \text{eV}\cdot\text{Å}\cdot e^{-2}$ with e , being the electron charge, A_{ij} and C_{ij} are parameters set according to each atom, r_{ij} is the distance between two pair of ions. For cation-cation pairs, only Coulombs interactions are sufficient so A_{ij} and C_{ij} are set to zero. For the NiFe₂O₄ spinel two different parameterizations (Buck-1, Buck-2) are found in literature [14,15,16] and presented in Table 2. The first one, Buck-1, uses partial charges 1.2 e , 1.8 e and -1.2 e for Ni, Fe and O respectively [14]. This pair potential form is proposed in Ref. [14], where it is used to investigate the structural properties of glasses and interfaces between glasses and spinel (MgAl₂O₄ and NiFe₂O₄) crystals through MD simulations. In that work, the authors add a correction short-range term at small distances to avoid unreasonable results caused by the Buckingham term, so this potential reads as

$$U_{ij}(r) = \begin{cases} \frac{z_i z_j e^2}{4\pi\epsilon_0 r_{ij}} + A_{ij} \exp\left(\frac{-r_{ij}}{\rho_{ij}}\right) - \frac{C_{ij}}{r_{ij}^6} & \text{if } r_{ij} \geq r_0, \\ \frac{z_i z_j e^2}{4\pi\epsilon_0 r_{ij}} + D_{ij} r_{ij}^2 + \frac{B_{ij}}{r_{ij}^n} & \text{if } r_{ij} < r_0, \end{cases} \quad (2)$$

where B_{ij} , D_{ij} and n are parameters fitted for each ion. A better choice could be the universal ZBL potential [29], which offers a more accurate description of short distance interactions (although it requires an intermediate spline interpolation between the two functions). This correction can be important in collisions where interactions at short distances are relevant, or in KMC simulations of diffusion of interstitial atoms where the closest distance between two pairs of atoms should be observed at saddle points, but for problems treated here like vacancy diffusion or computing of the elastic constants it can be safely ignored. The r_0 term is not given by the authors, but it can be easily computed using the Newton-Rapson method; this term is also given in Table 2.

The second parameterization, Buck-2, adopts formal charges of 2 e , 3 e and -2 e for Ni, Fe and O respectively and is taken from Ref. [15] (Ni²⁺-O²⁻ interactions) and Ref. [16] (Fe³⁺-O²⁻, O²⁻-O²⁻ interactions). The parameters are also given in Table 2.

In the case of magnetite Fe₃O₄, the Buckingham parameters Buck-3 are given in Table 2 where parameters for Fe³⁺O²⁻ and O²⁻O²⁻ interactions are the same as Buck-2. This parameterization has already been tested for vacancy diffusion in spinel systems in the temperature range from 1300 K to 2000 K and diffusion coefficients have been calculated from mean square displacements [16]. As before, Fe-Fe, Ni-Ni and Fe-Ni cation interactions are handled by a Coulomb term only.

2.2. Buckingham-Morse

Another potential proposed for the NFO spinel was conceived by adding a Morse term to the Buckingham potential [17]. This potential takes the form

Table 4

MEAM parameters for Ni, Fe, O: The cohesive energy E_c (eV), the equilibrium nearest neighbor distance r_e (Å), the exponential decay factor for the universal energy function α , the scaling factor for the embedding energy A , the exponential decay factors for the atomic densities $\beta^{(i)}$, the weighting factors for the atomic densities $t^{(i)}$ and the atomic density scaling ρ_0 .

	E_c	r_e	α	A	$\beta^{(0)}$	$\beta^{(1)}$	$\beta^{(2)}$	$\beta^{(3)}$	$t^{(0)}$	$t^{(1)}$	$t^{(2)}$	$t^{(3)}$	ρ_0
Ni	4.45	2.49	4.99	1.10	2.45	2.20	6.00	2.20	1.00	3.57	1.60	3.70	0.46
Fe	4.29	2.87	5.07	0.89	2.94	1.00	1.00	1.00	1.00	3.94	4.12	-1.50	0.90
O	4.59	1.21	4.59	0.80	2.31	2.26	2.07	1.52	1.00	11.80	8.40	-6.20	2.60

Table 5

MEAM potential parameters for mixed elements [2,18,31,33], reference structures are L_{12} (Ni₃Si type) and B_1 (NaCl type).

	Fe-Ni	Fe-O	Ni-O
Ref struct	L_{12}	B_1	B_1
Δ_{ij}	-0.0110	-1.3650	-1.2465
r_e	2.5031	2.1475	2.0842
α	5.2000	4.0000	4.1000
d	0.0	0.0	0.0

$$\Gamma = \sum_{i=1}^3 t^{(i)} \left(\frac{\rho^{(i)}}{\rho_0} \right)^2, \quad (8)$$

where $t^{(i)}$ are adjustable parameters and $\rho^{(i)}$ is the partial electron density as defined in Baskes [31,39]. Another possibility is

$$\rho = \rho_0 \sqrt{1 + \Gamma}, \quad (9)$$

however, according to Baskes, this form has the inconvenient that it yields imaginary electron densities for $\Gamma < 1$ which is possible if any of the $t^{(i)}$ are less than zero. We tested this form with Ni (labelled as MEAM-2) and with Ni and Fe (labelled as MEAM-3); O density is not changed. The results are almost identical for the stiffness constants but these representations have a significant impact on vacancy formation energies as will be shown in Section 4.5.

Two sets of parameters are required in the MEAM formalism. The first one has thirteen potential parameters for every unitary element (Ni, Fe, O) and they are listed in Table 4. The parameters r_e , E_c , α , are already explained above, A is the scaling factor for the embedding energy, $\beta^{(k)}$ are the exponential decay factors for the atomic densities and $t^{(k)}$ are the weighting factors for the atomic densities. In our LAMMPS implementation, we have used the default averaging rule for $t^{(i)}$ parameters.

The second set of parameters contains the information for the bonds Fe-Ni, Fe-O and Ni-O, as explained above, and are given in Table 5. In general, each bond requires approximately thirty independent parameters to describe the MEAM potential formalism. Most of them are the $C_{\min}(i, j, k)$ and $C_{\max}(i, j, k)$ many-body screening terms which are set to their default values of 2.0 and 2.8, because Ohira's parameterization is done for the 1NN-MEAM proposed by Baskes [31]. This approach reduced the number of parameters to three for each binary reference structure, E_{ij}^c , r_e , α or B (they can also be obtained from experiments or DFT works). We also fit the additional MEAM-LAMMPS-parameters to match the old version of DYNAMO code as described in the LAMMPS manual. The sublimation energy for a reference structure of a mixed type is defined by

$$E_{ij}^c = \frac{E_c^i + E_c^j}{2} - \Delta_{ij}, \quad (10)$$

where E_c^i is the sublimation energy of atom type i and Δ_{ij} (eV/atom) is the heat of formation of the reference structure, E_c^i or Δ_{ij} .

We test these parameterizations of Fe and O for the simulations of magnetite FO; in contrast to the Buckingham FO potential, the MEAM is not able to distinguish between Fe²⁺ or Fe³⁺ ion types; their distinction

is then only given by their occupation crystallographic site: tetrahedral (A) or octahedral (B).

3. Procedure

3.1. Sample construction

As stated in the introduction, ferrites are described by the general formula AB_2O_4 (see Appendix A for more details). For nickel-ferrite NFO, in the normal spinel case, Ni and Fe fill A and B sites respectively, in the inverse spinel the Fe atoms fill 8 A-sites and Ni and Fe fill randomly the 16B-sites. The case of the magnetite FO is similar. In a FO inverse spinel half of the Fe³⁺ ions occupy the cation tetrahedral A-sites and the rest (Fe²⁺ and Fe³⁺) occupy randomly the octahedral B-sites (the superscript is the charge used for Coulomb interactions). From the experimental viewpoint, the most chemically stable structure of NFO and FO is the inverse spinel structure. However, in this study, it has been considered important to analyze the behavior of the simulations of these compounds when their structures have a normal and inverse configuration.

Properties of a perfect crystal such as elastic constants, bulk modulus, shear modulus and cohesive energy are computed for each potential by using a $1 \times 1 \times 1$ -unit cell. This size is enough because periodic conditions produce images which substitute the need of a larger supercell. However, for vacancy formation energies a larger supercell of $10 \times 10 \times 10$ unitary cell is required to account for the effects produced by the stress associated with vacancy defects.

3.2. Minimization procedure

Minimizations can be done with the conjugate gradient (CG) algorithm or the Fast Inertial Relaxation Engine (FIRE) algorithm [40]. Both algorithms should properly stop a minimization when either energy or force tolerance is lower than a predefined value. The procedure to test our potentials is the following: first, for a given ideal spinel sample, the system is relaxed at a fixed lattice constant (chosen as the experimental one of 3.34 Å) to determine whether the system keeps the spinel structure. Second, we relax the system at constant zero pressure to obtain the relaxed lattice parameter. Third, elastic constants, bulk and shear modulus, cohesive energy and vacancy formation energies are computed for each potential with the lattice parameter obtained previously.

Long-range interactions can be handled via particle-particle particle-mesh (PPPM) or the Ewald methods [41] (the Wolf algorithm can be used [42,43], but the method exhibits poor performance). Computations of the elastic constants—in contrast to computation of the vacancy formation energy—are problematic because the algorithm depends on minimizations where not only the energy, but the force must be lower than predetermined tolerances. Relaxations that include this Coulombic part are problematic because simulations may stop before reaching the predefined force tolerance, i.e., the minimization procedure may stop because the algorithm is unable reduce the energy (from one step to the next one, the code stops if the change in energy is lower than the machine precision although the force is not yet lower than the tolerance). To avoid this problem, in the Ewald (or PPPM) sums, three parameters must be carefully chosen: the damping parameter α , the accuracy ϵ_{ewald} (the desired relative error in forces) and the cut of a distance r_c . For

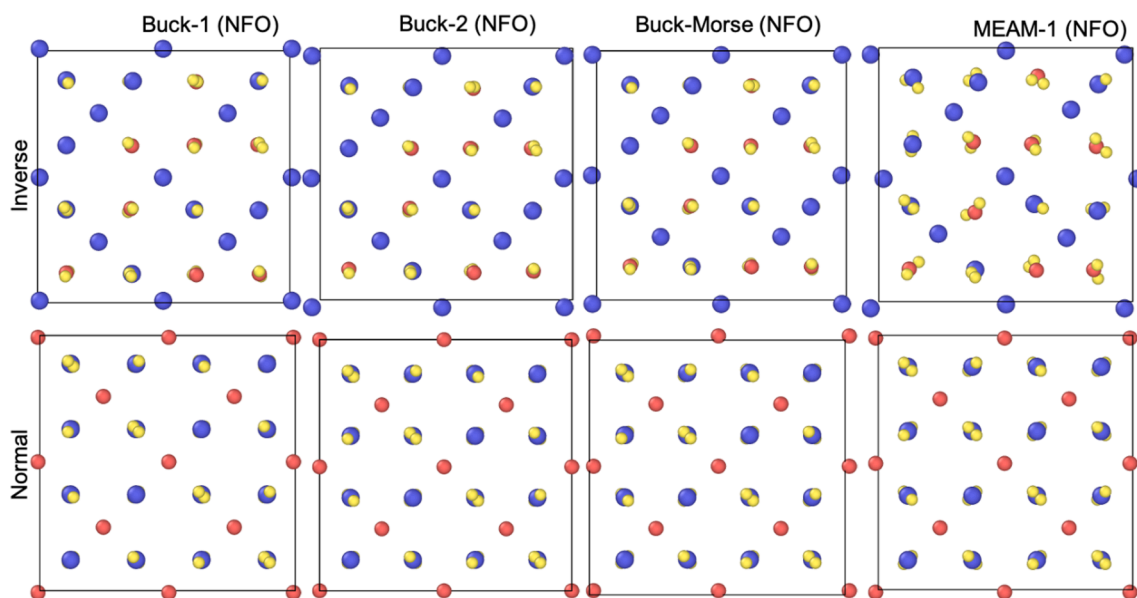


Fig. 1. Top view along the [100] direction of the inverse (top) and normal NFO-spinel (bottom) structures after relaxation at zero pressure using Buckingham, Buckingham-Morse, and MEAM potentials. Ni in blue, Fe in red, O in yellow. (For interpretation of the references to colour in this figure legend, the reader is referred to the web version of this article.)

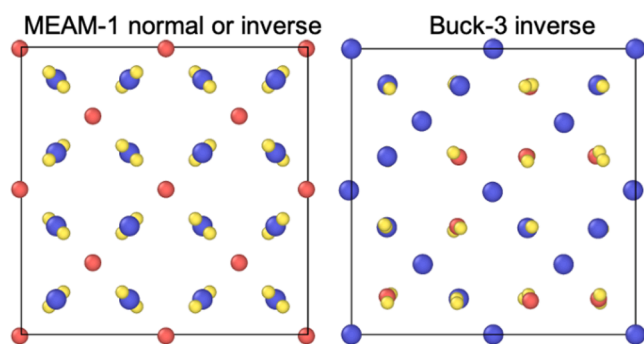


Fig. 2. Top view along the [100] direction of the inverse FO-spinel structure after relaxation at zero temperature and zero pressure using Buck-3 and MEAM-1 parameterizations. Fe²⁺ in blue, Fe³⁺ in red, O in yellow. (For interpretation of the references to colour in this figure legend, the reader is referred to the web version of this article.)

Table 6

Predicted anion parameters for normal NFO and FO spinels (Ideal is $u_{43m} = 0.375$).

Buck-1 (NFO)	0.385
Buck-2 (NFO)	0.388
Buck-Morse (NFO)	0.388
MEAM-1 (NFO)	0.390
MEAM-1 (FO)	0.389
Buck-3 (FO)	0.388

Buckingham and Buckingham-Morse potentials, a cut-off distance for computing long-range interactions into the k -space is set to $r_c = 16 \text{ \AA}$. Lower values show problems of convergence or do not recover the spinel structure. The precision for Buckingham is set to $\epsilon_{ewald} = 10^{-10}$ with Ewald method, this value is too small compared to usual values reported to be around $\sim 10^{-4}$ for MD simulations at other temperatures and larger box-sizes, however, minimizations here require more precision. In the case of the Buckingham-Morse, it performs better with PPPM and $\epsilon_{pppm} = 10^{-8}$. The damping parameter α is the predefined value computed by LAMMPS at the defined precision guarantying a full

relaxation for the unitary cell, then we keep this value for the larger systems. Adding the long-range term r^{-6} (via Ewald or PPPM) does not modify the results, so only r^{-1} is computed in the k -space. A force tolerance of 10^{-10} eV/\AA and energy tolerance of 0.0 eV is used in all minimizations, except in computations of vacancies formation energies where the energy tolerance is set to 10^{-5} eV .

4. Results and discussion

4.1. Geometries after minimizations

Fig. 1 and Fig. 2 show comparisons of the final structures obtained with different force fields after relaxation at zero pressure for the NFO and FO spinel systems; inverse (top) and normal (bottom). The geometry of the NFO normal spinel is maintained in all the simulations (Fig. 1). The MEAM-1 performs well for normal spinel and produces an acceptable distortion when tested with an inverse spinel (MEAM-2 and MEAM-3, which use the alternative density—see Section 2.3—, have similar results). Buckingham and MEAM predict similar geometries for FO normal spinels (Fig. 2). Fig. 2 presents Buck-3 and MEAM-1 structures for FO inverse a spinel; since MEAM does not handle charged ions, both normal and inverse spinels are represented with the same structure.

The anion parameters u associated with the potentials studied here—for both NFO and FO normal spinels—are systematically larger than the ideal value of $u_{43m} = 3/8$ [12]. However, as summarized in Table 6, all potentials generate anion parameters in good agreement with experiments. The increase in the value of u with respect to the ideal value u_{43m} is expected and associated with the movement of anions along the [111] direction outward from the nearest A-site, while the B-site volume is compressed and consequently its symmetry [44]. For NFO, Rietveld structure refinement gives values of 0.388 [11] and 0.380 [45], in agreement with our results. Similarly, in FO, a value of approximately 0.380(1) [46] is reported (here computed for normal spinel for simplicity), where the error depends on the size of the nanoparticles.

4.2. Bulk properties at zero pressure

Lattice parameter, energy and elastic constants for the normal and inverse spinels are summarized in Table 7 for NFO and Table 8 for FO

Table 7

Spinel NFO predicted data: lattice $a(\text{Å})$, energy/atom E_f (eV), bulk modulus B (GPa), rigidity (shear) modulus G (GPa), Young modulus E (GPa), Poisson ratio ν , elastic constants, C_{11} , C_{12} , C_{44} (GPa), anisotropic factor A and Debye temperature θ_D (K). Underlined are data computed from their elastic constants. Values in () mean that in one of directions lattice changes the last digit by that value. See Table 1 for a description of the potentials.

NFO-Normal	a	E_f	B	G	E	ν	C_{11}	C_{12}	C_{44}	A	θ_D
Buck-1	8.606	-10.843	164.57	78.28	195.97	0.30	235.69	129.00	94.83	1.78	580.5
Buck-2	8.415	-27.639	223.25	125.06	316.14	0.26	354.27	157.74	146.94	1.50	736.4
Buck-Morse	8.206	-12.156	206.39	69.48	187.41	0.35	254.09	182.54	108.13	3.02	547.9
MEAM-1	8.514	-7.041	142.82	78.84	199.77	0.27	244.94	91.76	80.38	0.38	588.3
MEAM-2	8.534	-7.032	144.35	81.97	206.77	0.26	252.82	90.11	82.38	1.01	600.2
MEAM-3	8.533	-7.040	143.93	80.34	203.21	0.26	251.73	90.03	80.00	0.99	594.4
NFO-Inverse	a	E_f	B	G	E	ν	C_{11}	C_{12}	C_{44}	A	θ_D
Buck-1 (Inv1)	8.58(7)	-10.862	174.56	72.15	190.23	0.32	233.81	144.78	99.73	2.24	568.5
Buck-1 (Inv2)	8.58(9)	-10.856	173.54	70.73	186.62	0.32	228.44	143.85	99.82	2.36	563.2
Buck-2 (Inv1)	8.31(2)	-27.609	247.22	121.58	313.54	0.29	354.33	195.15	161.52	2.03	723.9
Buck-2 (Inv2)	8.31(2)	-27.601	246.71	121.57	312.94	0.29	350.76	192.04	161.82	2.04	723.7
Buck-Morse (Inv1)	8.14	-12.306	216.29	96.21	251.27	0.31	311.34	167.83	117.09	1.63	638.6
Buck-Morse (Inv2)	8.13(4)	-12.298	215.55	95.35	249.13	0.31	308.59	167.45	116.64	1.65	635.5
MEAM-1 (Inv1)	8.2(3)	-7.040	120.43	79.66	195.56	0.23	217.81	70.5	83.93	1.14	578.9
MEAM-1 (Inv2)	8.2(3)	-7.044	135.27	79.18	196.14	0.24	219.83	77.64	85.08	1.20	577.9
Expt [14,49]	8.339	-	198.2	70.6	189.4	0.34	273.1	160.7	82.3/81[2]	1.46	556.3
DFT [50]	8.43/8.36[51]	-6.636[51]	177.1	76.17	199.85	0.31	252.2	139.5	93.2	1.65	578.6
MD-buck[14]	8.3	-	182.1	73.5	138.2	0.31	249.2	148.5	106.0	2.10	583.3
MD-MEAM[2,18]	8.342	-4.38	120	-	-	-	-	-	82	-	-

Table 8

Magnetite FO predicted data: lattice $a(\text{Å})$, energy/atom E_f (eV), bulk modulus B (GPa), rigidity (shear) modulus G (GPa), Young modulus E (GPa), Poisson ratio ν , elastic constants, C_{11} , C_{12} , C_{44} (GPa), anisotropic factor A and Debye temperature θ_D (K). The underline is data computed here from their elastic constants. Values in () means that in one of directions lattice changes the last digit by that value. MEAM-1 and MEAM-2 with Inv1 give the same data as Inv2.

FO-Inverse	a	E_f	B	G	E	ν	C_{11}	C_{12}	C_{44}	A	θ_D
MEAM-1 (Inv1)	8.570	-7.505	103.43	82.8mo0	196.07	0.18	233.04	38.62	74.37	0.77	603.0
MEAM-2 (Inv1)	8.600	-7.502	106.02	85.36	201.89	0.18	238.39	39.84	77.16	0.78	613.2
Buck-3 (Inv1)	8.34(5)	-27.486	240.71	119.88	308.62	0.29	347.17	189.05	158.47	2.00	724.4
Buck-3 (Inv2)	8.350(4)	-27.480	240.4	120.39	309.27	0.28	345.51	185.87	158.59	1.99	726.0
Expt [49]	8.396	-4.96[24]	159.6	89.3	225.8	0.26	267.6	105.6	95.3/97[2]	1.18	625.4
Expt [53,3]	8.396	-	185.7 ± 3.0	60.3 ± 3.0	163.3	0.35	260.5 ± 1.0	148.3 ± 3.0	63.3 ± 1.5	1.13	519.9
MD-MEAM[2]	8.399	-4.91	156	-	-	-	-	-	133	-	-
DFT [53]	-	-	187.4	48.99	135.19	0.38	242.3	159.9	55.0	1.33	470.3
DFT [54]	8.396	-	187.4	80.00	211.14	0.32	275 ± 40	155 ± 60	97 ± 13	1.62	596.1

and for each potential. Due to the random nature of the inverse spinel, two samples are used: Inv1 and Inv2. They are also compared to experimental and DFT results. The polycrystalline, bulk modulus B , Poisson ratio ν , rigidity modulus (or shear modulus) G , Young modulus E and the Zener anisotropy factor A , are calculated following the Voigt-Reuss-Hill scheme [47,48],

$$B = \frac{C_{11} + 2C_{12}}{3} \quad (11)$$

$$G = \frac{G_R + G_V}{2} \quad (12)$$

$$G_V = \frac{(C_{11} - C_{12}) + 3C_{44}}{5} \quad (13)$$

$$G_R = \frac{5(C_{11} - C_{12})C_{44}}{3(C_{11} - C_{12}) + 4C_{44}} \quad (14)$$

$$E = \frac{9GB}{G + 3B} \quad (15)$$

$$\nu = \frac{3B/2 - G}{G + 3B} = \frac{1}{2} \left(1 - \frac{3G}{3B + G} \right) = -1 + \frac{E}{2G} = \frac{3B - E}{6B} = \frac{1}{2} - \frac{E}{6B} \quad (16)$$

$$A = \frac{2C_{44}}{C_{11} - C_{12}} \quad (17)$$

According to Anderson [52], in an isotropic polycrystalline, the

Debye temperature θ_D can be approximated by

$$\theta_D = \frac{h}{k_B} \left[\frac{3nN_a\rho}{4\pi M} \right]^{1/3} v_m, \quad (18)$$

where $h/k_B = 4.7992431 \times 10^{-11}$ K-s, is the ratio of the Planck and Boltzmann constants, $n = 56$ is the number of atoms in the spinel, N_a is Avogadro's number, ρ is the density and M is the molecular weight. v_m is the average sound velocity given by

$$v_m = \left(\frac{1}{3} \left[\frac{2}{v_s^3} + \frac{1}{v_l^3} \right] \right)^{-1/3}, \quad (19)$$

$$v_s = \sqrt{\frac{G}{\rho}}, \quad v_l = \sqrt{\frac{B + 4/3G}{\rho}}, \quad (20)$$

where v_l and v_s are the longitudinal and shear (transverse) elastic sound velocities. Results for the Debye temperature predicted by each potential are also reported in Table 7 and Table 8.

For the NFO with Buck-1, we predict a lattice constant of ~ 8.6 Å (both normal and inverse spinels) and elastic constants of $C_{11} = 235$ GPa, $C_{12} = 129$ GPa, $C_{44} = 95$ GPa (see Appendix B for details of the computing). These results are slightly different from those reported in Ref. [14], where authors predict a lattice constant of 8.3 Å and elastic constants of $C_{11} = 249$ GPa, $C_{12} = 148$ GPa, $C_{44} = 106$ GPa. These differences may be due to a procedure not reported (DL_POLY and GULP codes are used in Ref. [14]), as we have repeated the computations with

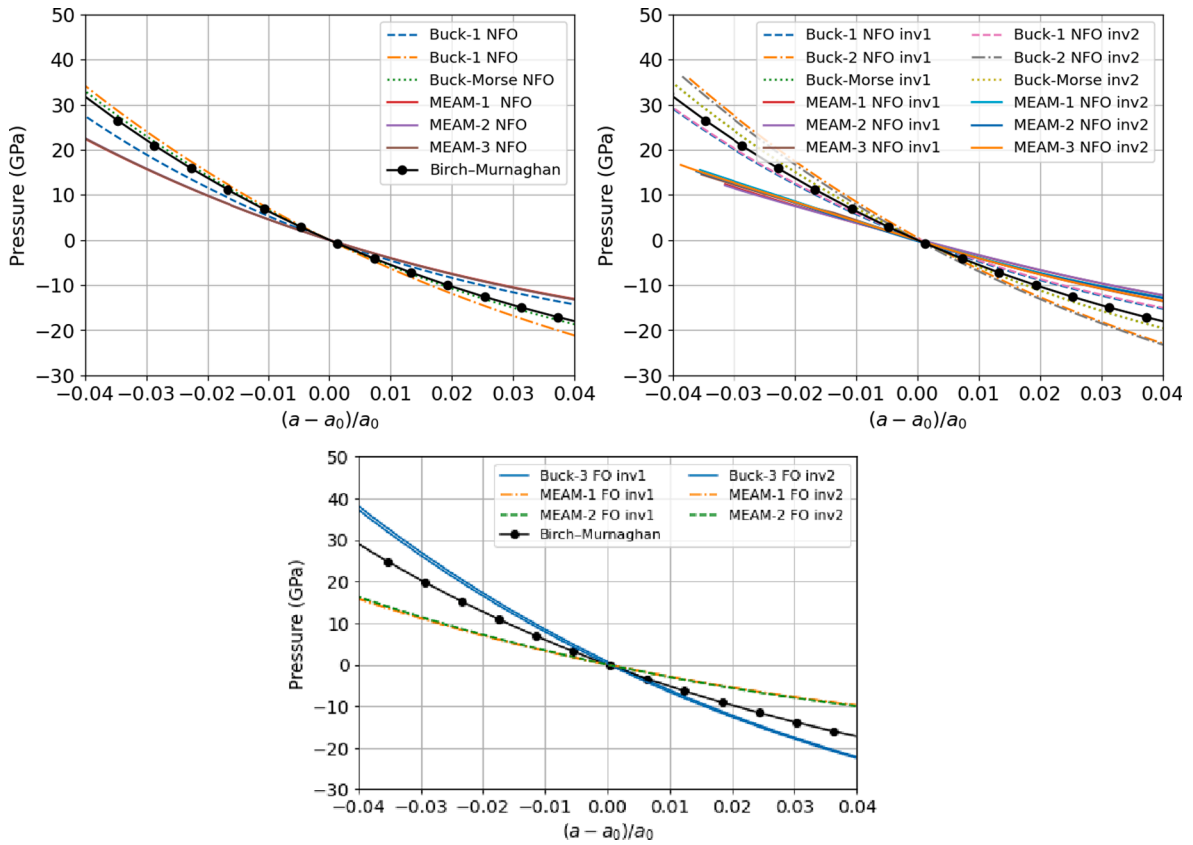


Fig. 3. Pressure as a function of the strain for a normal spinel NFO (top-left) and an inverse spinel (top-right). At the bottom magnetite FO spinel at zero temperature. Dotted lines are plots of the Birch-Murnaghan equation using experimental data of [Table 7](#) and [Table 8](#) with $B' = 4.0$.

GULP in the core-core approximation and have recovered the same LAMMPS results in contrasts to Ref. [14]. Our elastic constants differ somewhat, however, from experiment of Li [49]: the best agreement is found for C_{44} (relative error of $\sim 15\%$) and the bulk modulus (relative errors of $\sim 12\%$ in normal spinel and $\sim 17\%$ inverse).

The Buck-2 parameterization presents the largest difference when compared to experimental data. Its bulk modulus is $\sim 25\%$ above experiment for the inverse and $\sim 13\%$ above for the normal spinels (shear and young moduli are also larger).

For the NFO with Buck-Morse, the bulk modulus is $\sim 10\%$ higher than the experimental value for inverse spinel but $\sim 4\%$ higher for normal spinels. The shear and young moduli show larger discrepancies with the experiment and DFT, especially for inverse spinels (up to $\sim 27\%$ and $\sim 33\%$ larger than experiment). This is associated with the significant overestimation of C_{11} and C_{44} as compared to experimental results.

In general, both Buckingham and Buckingham-Morse potentials predict symmetrical normal-spinel structures where the components C_{11}, C_{12}, C_{44} are the only elastic constants different from zero. However, this is not the case for inverse spinel systems where the other elastic constants are not zero (although they are small, around ± 0.2 to ± 4 GPa). Also, the lattice parameter displays small differences (of up to 0.02 \AA) depending on the direction (x,y,z) . This is reported in [Table 7](#), where for one of the directions the last digit changes; e.g. in Buck-1, notation $a = 8.58(7) \text{ \AA}$ means that one of the lattice sizes the last digit changes from 8 to 7, i.e. after relaxation the unitary cell has a size of $8.58 \times 8.58 \times 8.57 \text{ \AA}$. This statistical “breaking of symmetry” is expected in “small” inverse systems and it is due to the random cation arrangement where two type of cations are randomly distributed in the octahedral sites and in contrast to a normal spinel where there is only one atom type in the octahedral sites; it vanishes for sufficiently large systems.

While magnetite FO is only observed as an inverse spinel in nature,

NFO crystallizes more commonly as an inverse spinel but can also form normal spinel. This is already predicted by Buck-1 and Buck-Morse parameterizations but Buck-2 fails as it predicts the opposite. Analogously, for the FO Buck-3, which shares the same parameters for Fe-O and O-O interactions, results are very similar to those of NFO with Buck-2 (see [Table 7](#)). In FO, depending on the experiment, C_{44} is found to be in the range from ~ 53 GPa to ~ 99 GPa [3], whereas the Buck-3 predicts ~ 158 GPa and the MEAM potentials predict on average ~ 75 GPa, which is more in agreement with the experiments or DFT.

Although we are unable to recover Ohira’s MEAM-1 results exactly with our implementation in LAMMPS (see MEAM in [Table 7](#)), our implementation gives the best overall results in NFO when compared with experimental and DFT data. However, the energy per atom, E_f , we find is around 60 % larger than Ohira’s. Nevertheless, it matches better with DFT prediction as it differs only by 6%. Furthermore, it is known that DFT tends to overestimate cohesive energies. The predicted elastic constants of the normal spinel fit better with the experimental results than those of the two inverse spinel samples. It seems that in Ohira’s work, the potential was fitted to a normal rather than an inverse spinel. Nevertheless, our results of inverse spinels are acceptable. The MEAM with inverse spinel is also affected by a random arrangement of Fe and Ni atoms in octahedral sites (elastic constants and bulk modulus etc), but the results are still in agreement with experimental data. Samples Inv1 and Inv2 give similar results. Thus, the shuffling of Fe and Ni atoms at octahedral sides gives randomness and we should expect an interval of error in all the stiffness quantities (although not computed here). However, the statistical error should disappear for systems large enough.

The Poisson ratio ν is proportional to the plasticity of materials and is therefore an indication of their stability. In the case of central forces, it is theoretically predicted that at zero pressure a material is stable if $0.25 < \nu < 0.50$, based on the requirement that the strain energy must

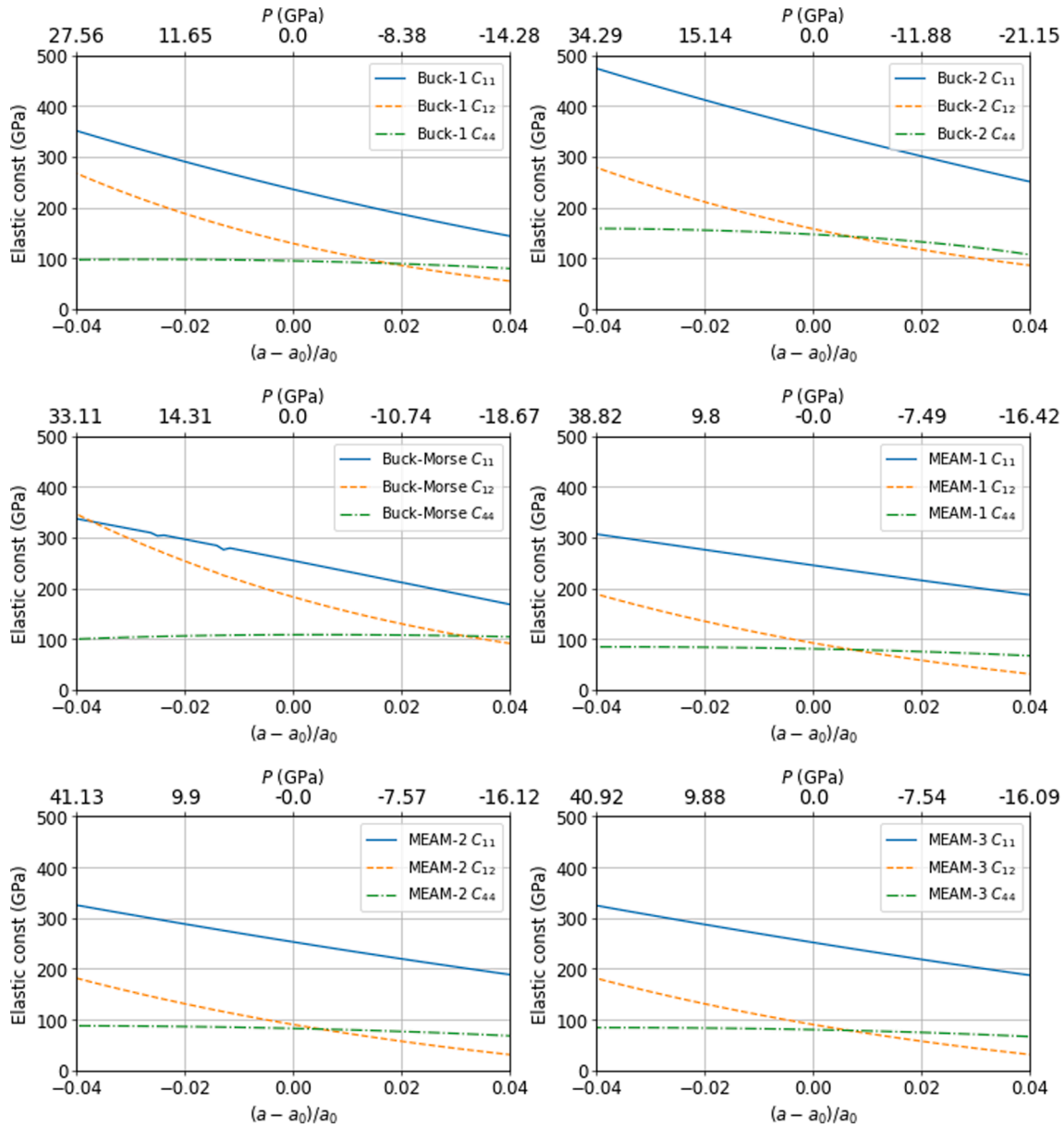


Fig. 4. Computation of the elastic constants at zero temperature for a normal NFO spinel as a function of the strain (bottom axis) and pressure P (top axis).

be positive [55,56]. This is indeed the case for the Buckingham potentials but not the case for the MEAM with inverse samples. Indeed, for NFO, the prediction is $\nu \approx 0.24$ which indicates that it is unstable; besides, the MEAM is not a central force due to the density term. In FO, the MEAM potentials predict too small $C_{12} \approx 39$ GPa and $\nu \approx 0.18$ compared to experiments, but the spinel is stable.

4.3. Pressure and elastic constants versus strain

It is important to know how a lattice change affects pressure and elastic constants. In the following simulations, pressure—computed as the average of the diagonal stress tensor, $P = (P_{11} + P_{22} + P_{33})/3$, see equation (26) in Appendix B—is plotted as a function of the strain by changing the lattice by a maximum of $\pm 4\%$ (or $\sim 12.5\%$ of volume) with respect to the zero pressure point, and relaxing the structure. We also compare to the Birch-Murnaghan equation of state written as function of lattice parameter [57,58],

$$P(a) = \frac{3B}{2} \left[\left(\frac{a_0}{a} \right)^7 - \left(\frac{a_0}{a} \right)^5 \right] \left\{ 1 + \frac{3}{4}(B' - 4) \left[\left(\frac{a_0}{a} \right)^2 - 1 \right] \right\}, \quad (21)$$

where B' is the derivative of the bulk modulus with respect to pressure, experimentally found to be 4 ± 0.4 for NFO and FO [57,58]. Experimentally, the bulk modulus, B , can be computed by least-squares fit of pressure–volume to the Birch-Murnaghan equation of state, here we rather use the experimental data of B, B' to plot $P(a)$ and compare (dots in Fig. 3). As before, the inverse spinel is tested with the two samples Inv1 and Inv2 and their plots are almost identical. Comparing the potentials, it is clear that while the Buckingham types have similar behavior (both normal and inverse spinels), with the MEAM types the lattice change produces a lower pressure (for instance, in the inverse spinel it is more than half compared to Buck-1 or Buck-Morse). There is no symmetry as pressure is higher for negative deformations (compression) than for positive deformations. All the Buckingham types predict a higher resistance to deformation of the lattice when tested with inverse spinel, in contrast to MEAM types that predict almost the half. For FO we observe similar results, the higher resistance to deformation is given by the Buckingham type in better agreement with the Birch-Murnaghan equation.

Elastic constants are computed as a function of the strain with results

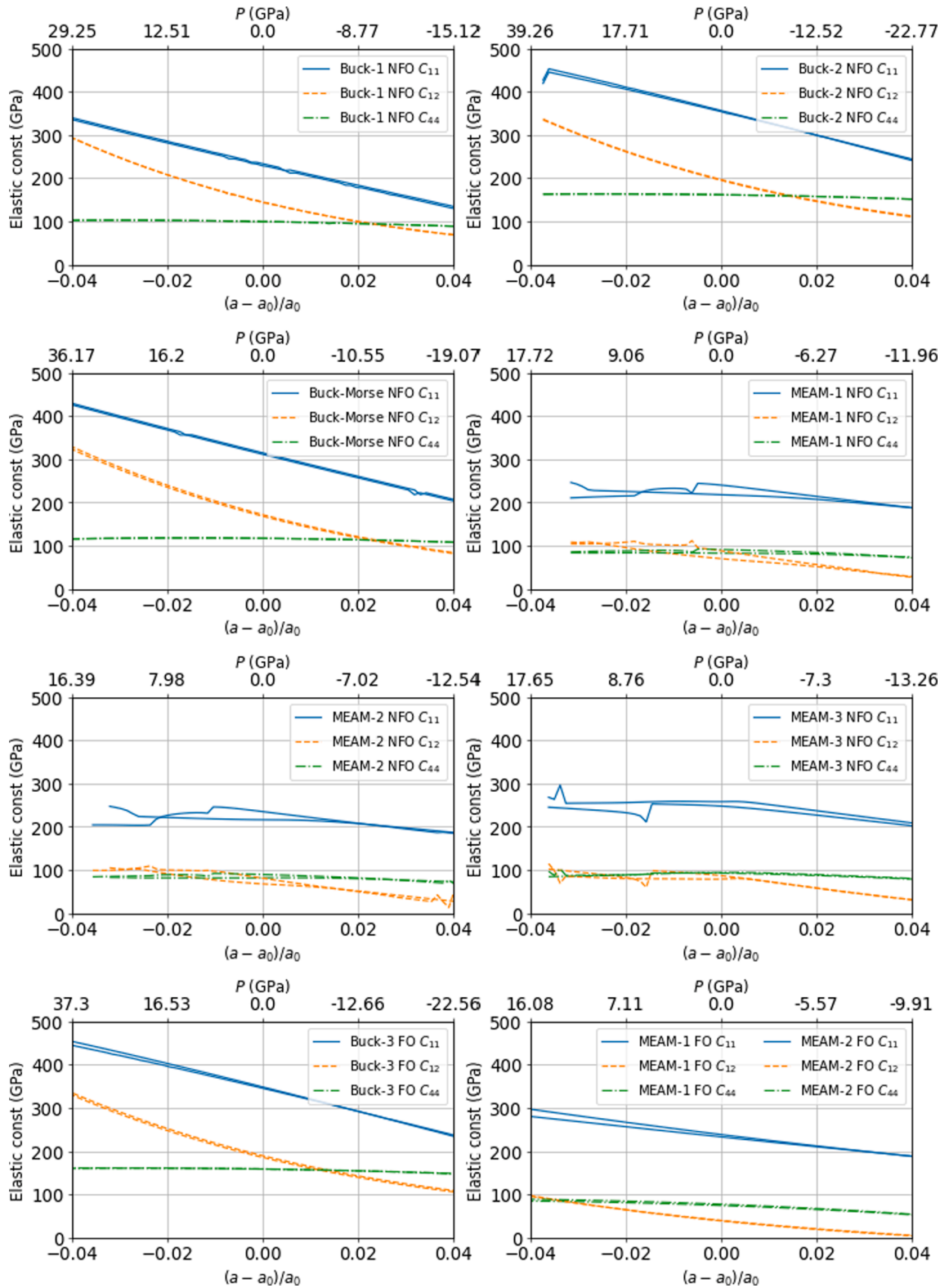


Fig. 5. Computation of the elastic constants at zero temperature for inverse NFO spinel and inverse FO (bottom) as a function of the strain (bottom axis) and pressure P (top axis).

shown in Fig. 4 and Fig. 5, for normal and inverse spinel structures respectively. The change in pressure is also shown on the top axis (for the inverse spinel, pressure is computed as the average of samples Inv1 and Inv2). In general spinel structures are mechanically stable if their elastic constants satisfy the following stability criteria [48]:

$$C_{11} > 0, \quad C_{44} > 0, \quad C_{11} > |C_{12}|, \quad (C_{11} + 2C_{12}) > 0. \quad (22)$$

Our calculations indicate thus that these criteria are indeed satisfied for all the potentials investigated here. Besides, we observe that the spinels are anisotropic with violation of Cauchy relation satisfied,

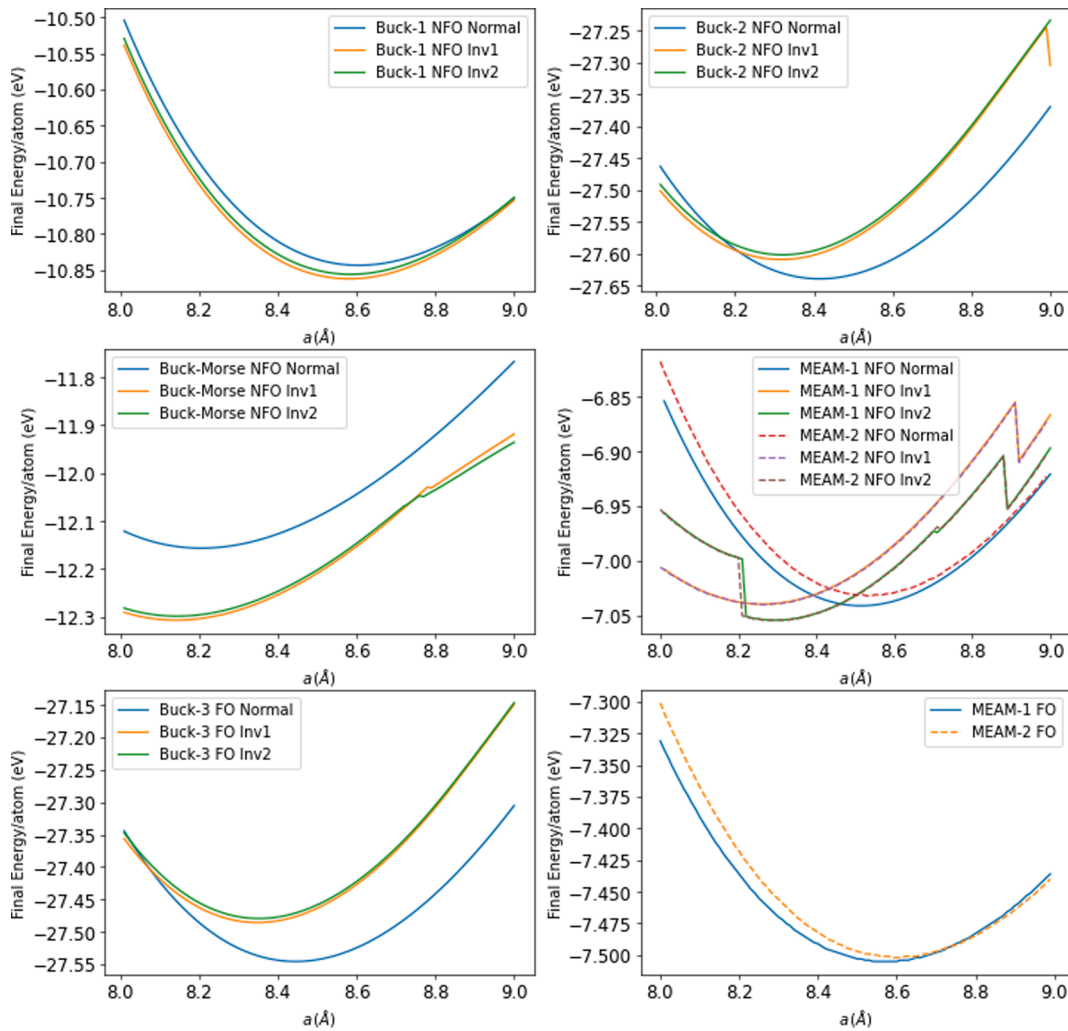


Fig. 6. Energy minimization as a function of the lattice a for NFO (top-center) and FO (bottom). Unitary cell sample with an energy tolerance of 0.0 eV and force tolerance of 10^{-10} eV. See Table 1 for a description of the potentials.

Table 9

Vacancy formation energies (eV) in normal-spinel structures NFO and FO, cubic box system of $10 \times 10 \times 10$ unitary cells.

Vacancy (NFO)	A-site	B-site	O
Buck-1	5.03	6.52	2.25
Buck-2	6.81	5.70	1.81
Buck-Morse	6.48	8.13	3.38
MEAM-1	1.57	-25.40	9.13
MEAM-2	1.60	-9.84	8.67
MEAM-3	1.58	-9.84	8.76
DFT-inverse [61]	0.52	1.56	-
Vacancy (FO)	Fe (A-site)	Fe (B-site)	O
Buck-3	6.29	8.19	3.33
MEAM-1	-2.27	-37.23	10.10

$C_{12} \neq C_{44}$. This is also manifested by the Zener anisotropic factor. It is also observed that, $C_{11} > C_{12} > C_{44}$, in all the cases except when MEAM-1 or MEAM-2 are used with the inverse samples, in that case, and in contrast to experiment, $C_{11} > C_{44} > C_{12}$. We see also that beyond the limits of ± 0.04 some potentials start to predict unstable structures, e.g., the Buck-Morse with a normal spinel start to predict that $C_{12} \gtrsim C_{11}$ under too much compression and in the case of Buck-2 we see that relaxations start to fail although stability criteria are still satisfied.

For NFO, in a normal spinel we observe that, for all potentials, C_{11} is

linear and all have approximately the same slope, in contrast to C_{12} , that is not linear and tends to grow faster with compression. C_{44} is approximately constant in all plots (although with Buck-2 or MEAM-1, it tends to decrease as box increases). For the inverse spinel, we observe similar results with Buckingham types, however, this is not the case for the MEAM types. For instance, under box compression the curves change their slope abruptly, indicating structural changes in the inverse spinel structure. Besides, depending on the sampled used (Inv1 or Inv2) C_{11} and C_{12} have different shapes, in contrast to C_{44} which is not affected. The Buck-1 is the only potential that predicts similar results for either normal or inverse spinel.

For FO, the Buck-3 potential gives similar results than Buck-2 with inverse spinels. In the case of MEAM-1 and MEAM-2 the results are similar, although the change of the density function produces a small variation of C_{11} . Under positive box expansion we see that these potentials predict that replacing Ni by Fe does not represent a big change for the mechanical properties. Experimental results in Ref. [3], predict a linear behavior as a function of the pressure up to 8 GPa for the components C_{11}, C_{12}, C_{44} , which are in agreement with our results.

4.4. Comparison of the minimum energies

To see the effects that the volumetric change produces in energy we performed a series of simulations as function of the lattice parameters a in the interval 8.0 Å to 9.0 Å (or equivalently, vary the volume from 512

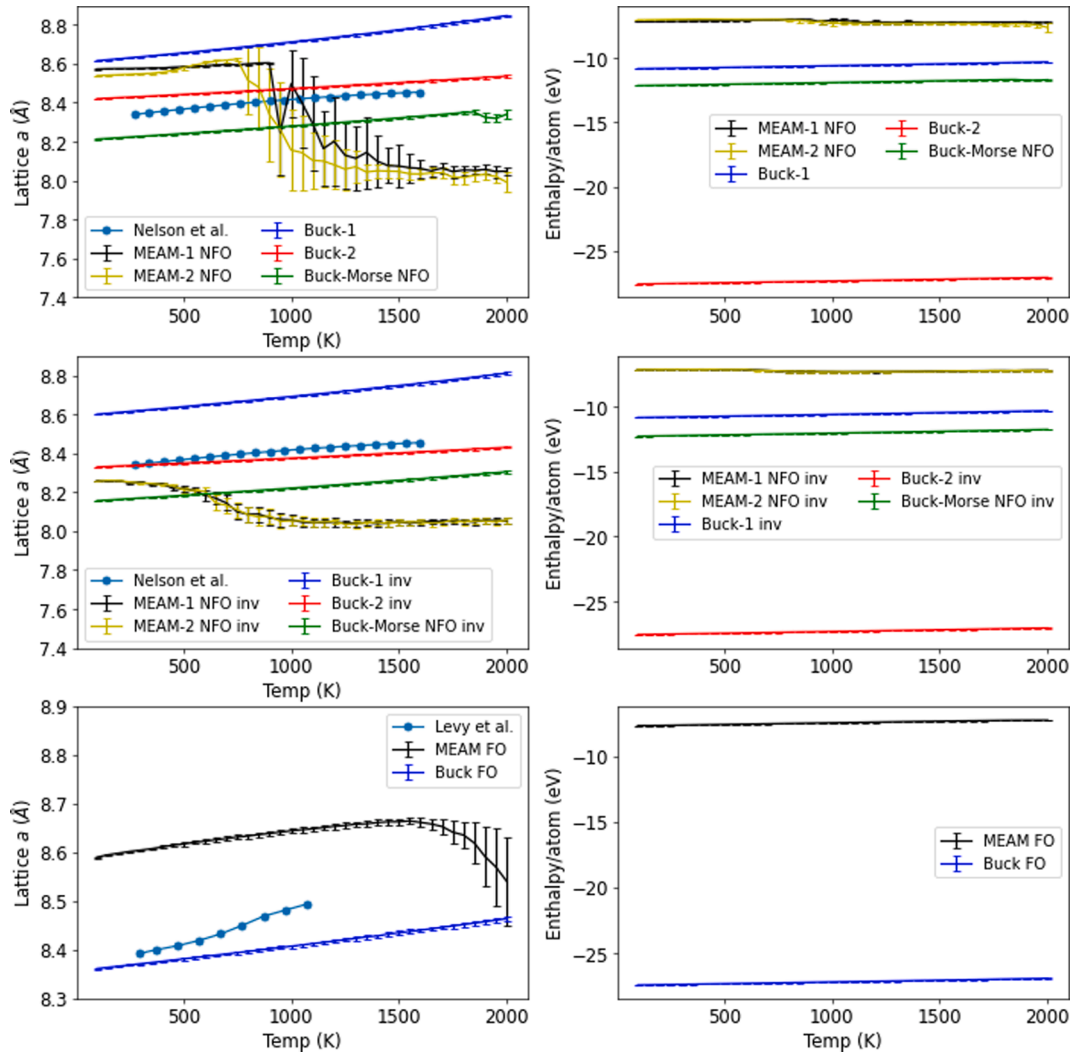


Fig. 7. Average lattice parameter, $a = \sqrt{V_x V_y V_z}$, (left) and enthalpy (right) as a function of temperature for normal NFO (top), inverse NFO (center) and inverse FO (bottom); data taken every 50 K. Averages taken every 2000 steps, first 50 000 steps are ignored. Dots are experimental data reported in Ref. [62,63].

Å^3 to 729 Å^3) with steps of 0.1 Å ; Fig. 6 shows the results. As before we used a normal and two inverse spinel samples (Inv1 and Inv2, although the results are similar, we see small variations of physical quantities).

Fig. 6 shows that for NFO the potentials Buck-1 and Buck-Morse predict the inverse spinel as the most stable structure in agreement with Ref. [59]. In contrast, Buck-2 and Buck-3 predict the normal NFO and FO spinels as the most stable structures and they have similar results as a consequence that both use the same parameters for Fe^{3+} and O^{2-} .

At zero pressure, Buck-1 and Buck-Morse predict a high cohesive energy of more than $\sim 10 \text{ eV/atom}$ (see Table 7), which is too large compared to experimental or DFT results of $\sim 5\text{-}7 \text{ eV/atom}$. It is worse for Buck-2 and Buck-3 (see Table 7 and Table 8), the total energies are more than twice than the energy predicted for Buck-1. This is a well-known problem of these coulombic potentials where a significant part of the interaction between the constituent ion arises from the Coulomb force between cations and anions at fixed charge [60]. The energy computed corresponds to the energy required to separate a crystal spinel into its individual ions as they no longer interact and, such a charged cloud has a significant Coulomb energy [60]. As a result, the lattice energy predicted by a fixed charge model is significantly higher than the experimentally measured cohesive energy, which is defined as the energy required to separate a crystal into individual neutral atoms [60]. Besides, these Buckingham models do not allow the simulations of different oxidation states or ensure charge neutrality in the crystal if the

cation and anion composition vary and it cannot be used to study the structure of the interface between a metal and its oxide. The change of nominal charges onto partial charges was also investigated for Buck-2 (and Buck-3) with similar results, but it predicts a larger lattice parameter of 10.2 Å , although this change reduces the energy of the unit cell to -8.34 eV/atom . Distortions at the end of some plots indicate the starting of loss of spinel structure due to the high pressure.

As can be observed in Fig. 6, for MEAM types, the energy only varies by around $\sim 0.2 \text{ eV}$ over the full interval. For NFO this potential performs better for normal than inverse structures. For instance, a small discontinuity (of around $\sim 0.05 \text{ eV}$) in the energy relaxation is evidenced for the inverse spinel sample Inv2, due to small distortions in the lattice positions, although the spinel structure is still preserved. This distortion indicates that the topology of the MEAM potential surface has some roughness, thus there exists at least two minima that are close and the code (CG or FIRE) minimizes to one if the lattice is lower than 8.2 Å and to the other if it is higher. Results as the final energy, lattice or elastic constants with MEAM (shown in Table 7), are not too much altered when the density is changed to the alternative density form $\rho = \rho_0 \sqrt{1 + \Gamma}$ (compare dashed lines-MEAM-2 to full lines-MEAM-1 in Fig. 6, MEAM-3 is not shown).

4.5. Ni, Fe and O vacancy formation energies

The vacancy formation energy E_V is the energy needed to create a vacancy defect in a perfect crystal, i.e., how much cohesive energy is needed to form a vacancy defect. For monoatomic systems it can be defined as

$$E_V = E'_t - \frac{N-1}{N}E_t, \quad (23)$$

where E'_t and E_t are the energies computed with and without a vacancy as obtained after a relaxation of spinel crystals with $(N-1)$ and N atoms. However, in ternary systems there are three different atomic types that contribute with different fractions to energy, thus this formula must be corrected to consider the fraction of each type

$$E_V = E'_i - \frac{N_i-1}{N_i}E_{i1} - E_{i2} - E_{i3}, \quad (24)$$

where E_{ii} are total energies by ion type i in the perfect crystal and N_i is the number of ions of type i where the vacancy is created, with $E_t = E_{t1} + E_{t2} + E_{t3}$ and $N = N_1 + N_2 + N_3$. For simplicity E_V is only computed for a normal spinel, the results are shown in Table 9. Buck-1 and Buck-2 predict similar results, but Buck-Morse predicts larger values. In contrast, the MEAM potentials predict negative formation energies, an unphysical result as it means that an imperfect structure with a vacancy is more stable than a perfect crystal. Yet, while these MEAM types seem to produce unphysical thermodynamic situation with respect to vacancy concentration, they predict stable structures under minimizations, which means that systems with defects can nevertheless be considered, with care, using these MEAM types. Besides, this also holds for finite temperature and especially for the MEAM-1 with FO system as corroborated in the next section.

4.6. Thermal effects on the lattice parameter at zero pressure

Finally, NPT simulations are done for temperatures from 100 K to 2000 K, in steps of 50 K, each simulation of 1 ns (1 million steps, each of 1 fs) with a box of $4 \times 4 \times 4$; the results are shown in Fig. 7. We also compare lattice to experiments (see dots) [62,63] (in the case of NFO, we use the reported fitting equation for the thermal expansion, α , to get $a = a_0(1 + \alpha\Delta T)$). The target pressure is set to zero, but it is well known that in NPT simulations pressure fluctuates. For instance, if Buck-1 is used, fluctuations vary from ~ 0.1 GPa at 100 K up to ~ 0.3 GPa at 2000 K and similarly for the MEAM, so we report the enthalpy per atom rather than the total energy. Buckingham type potentials predict stable structures as the temperature rises beyond 2000 K, however the experimental melting point of NFO is 1860 K [64]. The Buck-Morse potential starts to deform the normal spinel around that value, but it fails for the inverse spinel. The MEAM predicts that the normal spinel becomes unstable after 800 K (and 650 K for MEAM-2). The case of inverse spinel with MEAM is more critical, the structure starts deforming after ~ 300 K, meaning that this potential is unstable for NFO inverse spinel structures. However, the MEAM potential performs better for FO systems and the result is similar to the one found by the Buckingham potential. The MEAM FO predicts structure changes after ~ 1600 K while Buckingham does it after ~ 1800 K, close to the FO experimental melting point of 1856–1870 K [65,66]. Nevertheless, we emphasize that it is known that in general MD tends to overestimate the melting point, typically by up to 20% [67,68].

5. Conclusions

A literature research among the existing potentials for ternary Ni-Fe-O systems is done and a list of potentials useful for spinel ferrites NFO and FO is presented. Then, a comparison of static and dynamic bulk properties of these selected different empirical potentials, namely

Buckingham, Buckingham-Morse and MEAM is presented. Special attention is given to properties based on minimizations at zero temperature. For the description of the geometrical properties all the potentials behave acceptably well, e.g., the anion parameters predicted are in good agreement with DFT and experimental observations. Under induced pressure, Buckingham types offer more stability than the MEAM types (in the interval studied —up to $\pm 4\%$ lattice variation— all the potentials predict stable spinel structures). For the elastic constants, depending on the potential, acceptable differences can be observed when comparing to DFT and experimental reports. It is found that in an inverse spinel the occupancy order in octahedral sites affects the elastic constants.

For NFO systems: the Buckingham potentials with Buck-1 and Buck-2 parameterizations reproduce the known problem of predicting very high cohesive energies even though they reproduce the right geometry. Buck-1, for its part, correctly predicts the inverse spinel as the most stable structure, in contrast to Buck-2 which predicts the contrary. Furthermore, the Buck-2 cohesive energy is more than two times larger than the Buck-1 (due to the use of full charges). Also, its Debye temperature prediction is too large compared to experiment (in part because C_{44} is too large). Buck-Morse correctly predicts that the inverse spinel is the most stable structure and the cohesive energies are similar to those predicted by Buck-1. In this case, the prediction of elastic constants and derived bulk properties are better than Buck-2 but worse than Buck-1. During energy minimizations, the MEAM variants are good for normal-NFO spinels, as it has the best behavior of all at zero pressure and the elastic constants have the best agreement with DFT and experimental results. However, at higher temperatures the normal spinel becomes unstable and the structure is lost if the temperature is superior to 800 K for MEAM-1 or 650 K for MEAM-2. The MEAM potentials fail with inverse spinel structures, as they are unstable if temperature is different from zero. That instability could be a consequence of the lack of a long range term. The MEAM variants fail to correctly predict the vacancy formation energies, nevertheless they produce stable structures for NPT simulations of crystals without defects.

For FO systems: MEAM potentials perform well but their main failure is the impossibility to distinguish charge allotropes of iron (Fe^{2+} or Fe^{3+}). Despite the fact that the MEAM potentials predict too small C_{12} of ~ 39 GPa and small Poisson's ratio of 0.18 compared to experiments, the potential seems to be stable at higher temperatures. This is a consequence of the embedded energy, which makes the potential non-central. It also fails to correctly predict vacancy formation energies. Despite this issue, NPT simulations with crystals without defects up to 1 ns and up to 2000 K, predict stable structures. Buck-3 for FO predicts that the normal spinel is more stable than the inverse, although the FO normal spinel does not exist in nature. For the elastic constants and derived bulk properties, Buck-3 predicts too large values (e.g. it has the largest Debye's temperature prediction).

In general, for FO we recommend MEAM for general cases where speed is required but no distinction between normal or inverse is demanded. For NFO we only recommend MEAM for static or low-temperature simulations with a perfect normal spinel. However if this is not the case, the Buckingham types are the best option but they can be up to ten times more computationally costly. In any case care should be taken with defects.

Finally, more research to find new empirical potentials that better describe the bulk properties of spinel systems of FO and NFO is still needed because, as shown in this paper, each potential discussed here give only a partial description of the structure.

CRediT authorship contribution statement

Óscar A. Restrepo: Investigation, Conceptualization, Methodology, Software, Data curation, Writing – original draft, Visualization. **Óscar Arnache:** Validation, Writing – review & editing. **J. Restrepo:** Validation, Writing – review & editing. **Charlotte S. Becquart:** Validation,

Writing – review & editing. **Normand Mousseau:** Validation, Writing – review & editing, Cluster resources.

Declaration of Competing Interest

The authors declare that they have no known competing financial interests or personal relationships that could have appeared to influence the work reported in this paper.

Acknowledgements

This work was supported in part by grants from the Natural Sciences

and Engineering Research Council of Canada (NSERC). We are grateful to Calcul Québec/Compute Canada (CQ/CC) for generous allocations of computer resources. J. R. acknowledges University of Antioquia for the exclusive dedication program and the CODI-UdeA 2020-34211 project. O. Arnache wants to thank for the financial support by Solid State Group - GES at the University of Antioquia in the framework of Sustainability Strategy 2020-2021 and by Colombian ministry of science and technology - Minciencias (project no. 111580863381, contract 325-2019 - Acta CODI-2019-25990).

Appendix A. Spinel Geometry

In general, the detailed atomic arrangements in a spinel unitary cell is described by three structural parameters: first, the lattice parameter, a ; second, the anion parameter, u ; and third, the cation inversion parameter, i . More exactly, for cations X and Y, the spinel chemical formula can be written as follows [12],

$$(Y_i^{q+} X_{1-i}^{p+}) [X_{i/2}^{q+} Y_{(2-i)/2}^{p+}]_2 O_4, \tag{25}$$

where () and [] denote A and B sites respectively. The variable i is the inversion parameter and it specifies the fraction of A-sites occupied by majority ions. For normal spinel, $i = 0$; for random cation arrangement, $i = 2/3$, and for inverse spinel, $i = 1$ (here we limit our study to normal and inverse system only). The ideal unitary cell sample is shown in Fig. 8 for two different representations: on top, with origin at $\bar{4}3m$ point symmetry and, on bottom, at $\bar{3}m$, where $u_{\bar{4}3m} = 3/8 = 0.375$ and $u_{\bar{3}m} = 1/4 = 0.250$ respectively and they differs by a simple translation, $u_{\bar{4}3m} = u_{\bar{3}m} + 1/8$. According to the conclusions of Ref. [12], the lattice parameter a should depend on the average effective cation radius and without significant dependence on the specific cation arrangement, but u should be highly dependent on the cation inversion parameter i . Thus, in order to predict anion parameters in spinels, prior knowledge of the cation arrangement is required. Good empirical potentials for spinels should be able to describe also this fact.

For comparing the geometries found with the different potentials, we look at the radial distribution function (RDF), which is shown in Fig. 9. In the interval $[0, a]$ there are 22 different peaks; only the first five are described: The first peak are the four nearest AO neighbors distances ($\sqrt{3}a/3$) forming a tetrahedral site and the second peak, the six nearest BO neighbors distances ($a/4$), forming an octahedral site. The third peak are second nearest neighbors distances BB ($\sqrt{2}a/4$) (same distance than OO), The four peak are second nearest neighbors distances AB and AO ($\sqrt{11}a/8$). The fifth peak are AA and second neighbors BO distances ($\sqrt{3}a/4$).

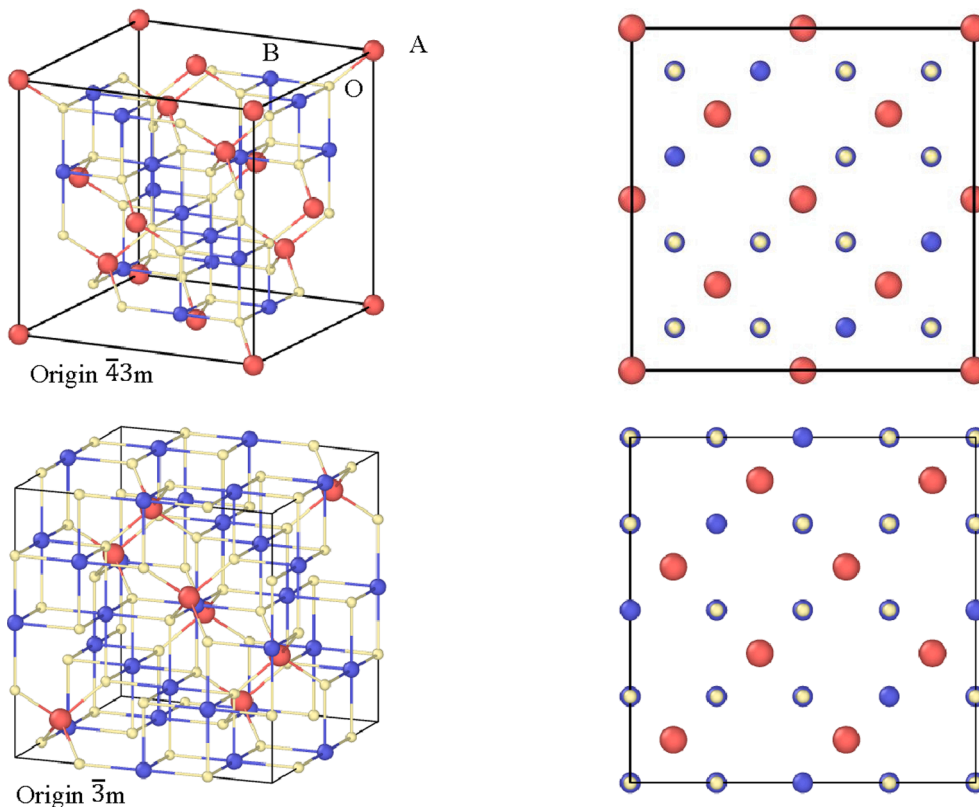


Fig. 8. Description of the ionic positions in spinel depends on the choice of the origin in the $Fd\bar{3}m$ space group. Two different equipoints with point symmetries $\bar{4}3m$ (on top) and $\bar{3}m$ (on bottom) are possible choices for the unit-cell origin [12]. AB_2O_4 has 8 tetrahedral cations A (red), 16 octahedral B cations (blue) and 32 anions (yellow). In left the corresponding top view images on (100) direction. (For interpretation of the references to colour in this figure legend, the reader is referred to the web version of this article.)

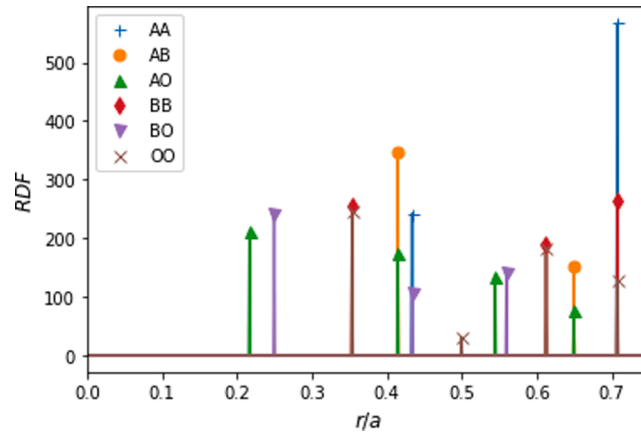


Fig. 9. RDF of an ideal A_2BO_4 spinel. First two peaks (at distances $\sqrt{3}a/8$ and $a/4$) are first nearest neighbors to A and B sites and the next three, have their second nearest neighbors distances at: $\sqrt{2}a/4$, $\sqrt{11}a/8$, $\sqrt{3}a/4$.

Table 10

Fractional coordinates of ideal lattice sites in the cubic unit cell of spinel in the Wyckoff notation. A-cation sites (point symmetry $\bar{4}3m$), B-cation sites (point symmetry $\bar{3}m$) and X-anion sites (point symmetry $3m$).

Origin at $\bar{4}3m$ A-site cation, $u = 3/8$.	Origin on inversion center $\bar{3}m$, $u = 1/4$.
A = $[0, 0, 0]$, $[\frac{1}{4}, \frac{1}{4}, \frac{1}{4}]$, two sites.	A = $[\frac{1}{8}, \frac{1}{8}, \frac{1}{8}]$, $[\frac{7}{8}, \frac{7}{8}, \frac{7}{8}]$, two sites.
B = $[\frac{5}{8}, \frac{5}{8}, \frac{5}{8}]$, $[\frac{5}{8}, \frac{7}{8}, \frac{7}{8}]$, $[\frac{7}{8}, \frac{5}{8}, \frac{7}{8}]$, $[\frac{7}{8}, \frac{7}{8}, \frac{5}{8}]$, four sites.	B = $[\frac{1}{2}, \frac{1}{2}, \frac{1}{2}]$, $[\frac{1}{2}, \frac{1}{4}, \frac{1}{4}]$, $[\frac{1}{4}, \frac{1}{2}, \frac{1}{4}]$, $[\frac{1}{4}, \frac{1}{4}, \frac{1}{2}]$, four sites.
X = $[u, u, u]$, $[\frac{1}{4}-u, \frac{1}{4}-u, \frac{1}{4}-u]$, eight sites.	X = $[u, u, u]$, $[-u, -u, -u]$, eight sites.
$[u, -u, -u]$, $[\frac{1}{4}+u, \frac{1}{4}+u, \frac{1}{4}-u]$,	$[u, (\frac{1}{4}-u), (\frac{1}{4}-u)]$, $[(\frac{1}{4}-u), u, (\frac{1}{4}-u)]$,
$[-u, u, -u]$, $[\frac{1}{4}+u, \frac{1}{4}-u, \frac{1}{4}+u]$,	$[(\frac{1}{4}-u), (\frac{1}{4}-u), u]$, $[-u, (\frac{3}{4}+u), (\frac{3}{4}+u)]$,
$[-u, -u, u]$, $[\frac{1}{4}-u, \frac{1}{4}+u, \frac{1}{4}+u]$.	$[(\frac{3}{4}+u), -u, (\frac{3}{4}+u)]$, $[(\frac{3}{4}+u), (\frac{3}{4}+u), -u]$.

The conventional choices for the unit-cell origin in spinel are either $\bar{4}3m$, on an A-site cation or $\bar{3}m$ on an octahedral vacancy (the latter is an inversion center). Table 10 lists the fractional coordinates of the spinel cubic unit cell for two choices. The spinel has a fcc unitary cell with coordinates (0,0,0) and $a(0.5,0.5,0.5)$, the unitary cell is simply created by adding to these points the fractional coordinates.

Appendix B. Elastic constants

The computational procedure is implemented as a script in the LAMMPS examples. The six stress components are calculated from a summation over all N particles in the system [69,70],

$$P_{ij} = \frac{1}{V} \sum_{k=1}^N m_k v_{ki} v_{kj} + \frac{1}{V} \sum_{k=1}^N r_{ki} f_{kj}, \quad (26)$$

with i and $j = x, y, z$. The r_{ki} , v_{ki} and f_{ki} are the vector components in the direction i of the position, velocity and force for the atom k . N means that the simulation includes periodic image atoms outside the central box because periodic boundary conditions are used. The first sum is zero because, $v_{ki} = 0$, in minimizations. This gives a symmetric pressure tensor, stored as a 6-element vector, with the components ordered by xx, yy, zz, xy, xz, yz .

Elastic constants are related to the stress tensor by the relation $C_{\alpha\beta} = -\frac{\partial P_\alpha}{\partial e_\beta}$, where e_β is the strain tensor and α, β stands for $1 \rightarrow 11 = xx$, $2 \rightarrow 22 = yy$, $3 \rightarrow 33 = zz$, $4 \rightarrow 23 = yz$, $5 \rightarrow 13 = xz$, $6 \rightarrow 12 = xy$ values (in Voigt notation). At zero temperature, these derivatives can be estimated by deforming the simulation box in one of the six directions and measuring the change in the stress tensor P_α . The first step is to minimize the system to get zero pressure and compute the stress tensor, P_α^0 . Then, the unitary cell is deformed by a small positive fraction Δ_α and minimized again to get the stress tensor after the deformation $P_\alpha^f = P_\alpha(\Delta_\alpha)$. Then, the derivatives with respect to strain components e_β can be computed using finite differences

$$C_{\alpha\beta}^+ = -\Delta P_\alpha / \Delta e_\beta = -(P_\alpha^f - P_\alpha^0) / h, \quad (27)$$

where $\Delta e_\beta \approx h l_i / l_j = h$, as the box is a square. The l_i are the box sizes, l_x, l_y, l_z , and $h = 10^{-6}$ is the finite deformation size (we should try several values of h to verify that results do not depend on it). This procedure is repeated for a small negative fraction deformation so

$$C_{\alpha\beta}^- = (P_\alpha^f - P_\alpha^0) / h. \quad (28)$$

More exactly, $C_{\alpha\beta}^{\pm}$ are computed after deforming the simulation box by, Δ_{α} , in the six directions, ($\alpha = 1, \dots, 6$)

$$\begin{aligned} C_{\alpha 1}^{\pm} &= \mp [P_{\alpha}(\Delta_x = \pm h l_x) - P_{\alpha}^0]/h \\ C_{\alpha 2}^{\pm} &= \mp [P_{\alpha}(\Delta_y = \pm h l_y) - P_{\alpha}^0]/h \\ C_{\alpha 3}^{\pm} &= \mp [P_{\alpha}(\Delta_z = \pm h l_z) - P_{\alpha}^0]/h \\ C_{\alpha 4}^{\pm} &= \mp [P_{\alpha}(\Delta_{yz} = \pm h l_z) - P_{\alpha}^0]/h \\ C_{\alpha 5}^{\pm} &= \mp [P_{\alpha}(\Delta_{xz} = \pm h l_x) - P_{\alpha}^0]/h \\ C_{\alpha 6}^{\pm} &= \mp [P_{\alpha}(\Delta_{xy} = \pm h l_y) - P_{\alpha}^0]/h, \end{aligned} \quad (29)$$

where (\pm) are positive or negative deformations. Next, an average is taken for each of the six components, i.e., the elastic constants are computed as, $C_{\alpha\beta} = (C_{\alpha\beta}^+ + C_{\alpha\beta}^-)/2$. By symmetry it must be demanded that $C'_{12} = (C_{12} + C_{21})/2$, $C'_{13} = (C_{13} + C_{31})/2$ and $C'_{23} = (C_{32} + C_{23})/2$, and finally the average moduli for cubic crystals is computed

$$\begin{aligned} C_{11} &= \frac{C_{11} + C_{22} + C_{33}}{3}, \\ C_{12} &= \frac{C'_{12} + C'_{13} + C'_{23}}{3}, \\ C_{44} &= \frac{C_{44} + C_{55} + C_{66}}{3}. \end{aligned} \quad (30)$$

Because the spinel system is a cubic crystal it must be satisfied that

$$\begin{aligned} C_{11} &= C_{22} = C_{33}, \\ C_{12} &= C_{13} = C_{23}, \\ C_{44} &= C_{55} = C_{66}, \end{aligned} \quad (31)$$

the rest of coefficients must be zero, that is, an ideal spinel is a cubic crystal system where the elastic modulus matrix can be written as follows

$$C = \begin{bmatrix} C_{11} & C_{12} & C_{12} & 0 & 0 & 0 \\ C_{12} & C_{11} & C_{12} & 0 & 0 & 0 \\ C_{12} & C_{12} & C_{11} & 0 & 0 & 0 \\ 0 & 0 & 0 & C_{44} & 0 & 0 \\ 0 & 0 & 0 & 0 & C_{44} & 0 \\ 0 & 0 & 0 & 0 & 0 & C_{44} \end{bmatrix} \quad (32)$$

This method constitutes a generic manner to obtain the elastic constants for any potential.

Appendix C. Supplementary material

Supplementary data to this article can be found online at <https://doi.org/10.1016/j.commatsci.2022.111653>.

References

- [1] Hoppe Michael, Magnetic, Structural, and Electronic Properties of NiFe2O4 Ultrathin Films, Schriften Des Forschungszentrums Jülich Reihe Schlüsseltechnologien, Band 118. Jülich: Forschungszentrum Jülich, 2016, ISBN 978-3-95806-122-4.
- [2] T. Ohira, Y. Inoue, K. Murata, J. Murayama, Appl. Surf. Sci. 171 (2001) 175.
- [3] H.J. Reichmann, Steven D. Jacobsen, Am. Mineral. 89 (2004) 1061–1066.
- [4] H. Salazar-Tamayo, K.E.G. Tellez, C.A.B. Meneses, Mat. Res. 22 (2019), e20190298.
- [5] I. Tsiachristos, et al., EPJ Web Conf. 75 (2014) 06005.
- [6] J.Y. Cheong, S. Lee, J. Lee, H. Lim, S. Cho, D.C. Lee, I. Kim, RSC Adv. 9 (2019) 27257.
- [7] M.M. Mujahid, et al., Ceram. Int. 45 (2019) 8486.
- [8] E.K. Heidari, B. Zhang, M.H. Sohi, A. Ataie, J.-K. Kim, J. Mater. Chem. A 2 (2014) 8314.
- [9] Y. Zhang, W. Cao, Y. Cai, J. Shu, M. Cao, Inorg. Chem. Front. 6 (2019) 961.
- [10] N. Rezlescu, E. Rezlescu, C. Doroftei, P.D. Popa, J. Phys.: Conf. Ser. 15 (2005) 296.
- [11] S.M. Patange, S.E. Shirsath, G.S. Jangam, K.S. Lohar, S.S. Jadhav, K.M. Jadhav, J. Appl. Phys. 109 (2011), 053909.
- [12] K.E. Sickafus, J.M. Wills, N.W. Grimes, J. Am. Ceram. Soc. 82 (2004) 3279.
- [13] H. Salazar-Tamayo, K.E. García, C.A. Barrero, J. Magn. Magn. Mater. 471 (2019) 242.
- [14] W. Sun, J. Du, J Am Ceram Soc 102 (2019) 4583.
- [15] P.M. Oliver, G.W. Watson, S.C. Parker, Phys. Rev. B 52 (1995) 5323.
- [16] J. Vaari, Solid State Ionics 270 (2015) 10.
- [17] A. Chartier, B. Golovchuk, S. Gossé, L. Van Brutzel, J. Chem. Phys. 139 (2013), 134702.
- [18] T. Ohira, Y. Inoue, Mat. Res. Soc. Symp. Proc. 492 (1998) 401.
- [19] X.W. Zhou, H.N.G. Wadley, J. Phys.: Condens. Matter 17 (2005) 3619.
- [20] Lee, webpage: <https://cmse.postech.ac.kr/home>.
- [21] C. Wu, B.-J. Lee, X. Su, Calphad 57 (2017) 98.
- [22] E. Lee, K.-R. Lee, M.I. Baskes, B.-J. Lee, Phys. Rev. B 93 (2016), 144110.
- [23] E. Lee, K.-R. Lee, B.-J. Lee, Comput. Mater. Sci. 142 (2018) 47.
- [24] J. Byggmästar, M. Nagel, K. Albe, K.O.E. Henriksson, K. Nordlund, J. Phys.: Condens. Matter 31 (2019), 215401.
- [25] J.D. Gale, JCS Faraday Trans. 93 (1997) 629.
- [26] D. Chicot, J. Mendoza, A. Zaoui, G. Louis, V. Lepage, F. Roudet, J. Lesage, Mater. Chem. Phys. 129 (2011) 862.
- [27] S. Plimpton, J. Comput. Phys. 117 (1995) 1.
- [28] X. Yu, Z. Zhan, J. Rong, Z. Liu, L. Li, J. Liu, Chem. Phys. Lett. 600 (2014) 43.
- [29] J.F. Ziegler, J.P. Biersack, U. Littmark. In The Stopping and Range of Ions in Matter, volume 1, New York, 1985. Pergamon. ISBN 0-08-022053-3.
- [30] H. Fang, P.M. Gullett, A. Slepoy, M.F. Horstemeyer, M.I. Baskes, G.J. Wagner, M. Li, Numerical Tools for Atomistic Simulations, Sandia National Laboratories, 2004.
- [31] M.I. Baskes, Modified Embedded Atom Method Calculations of Interfaces, Sandia National Labs, Livermore, CA (United States), 1996.
- [32] M.S. Daw, M.I. Baskes, Phys. Rev. B 29 (1984) 6443.
- [33] M.I. Baskes, Phys. Rev. B 46 (1992) 2727.
- [34] B. Lee, Phys. Rev. B 62 (2000) 8564.
- [35] B. Lee, Kim Cho, Phys. Rev. B 64 (2001), 184102.
- [36] G. Wang, M.A. Van Hove, P.N. Ross, M.I. Baskes, J. Chem. Phys. 121 (2004) 5410.
- [37] J.H. Rose, J.R. Smith, F. Guinea, J. Ferrante, Phys. Rev. B 29 (1984) 2963.
- [38] F. Kong, R.C. Longo, C. Liang, D.-H. Yeon, Y. Zheng, J.-H. Park, S.-G. Doo, K. Cho, Comput. Mater. Sci. 127 (2017) 128.
- [39] M.I. Baskes, Mater. Chem. Phys. 50 (1997) 152.
- [40] E. Bitzek, P. Koskinen, F. Gähler, M. Moseler, P. Gumbsch, Phys. Rev. Lett. 97 <https://doi.org/10.1103/PhysRevLett.97.170201>.
- [41] C.J. Fennell, J.D. Gezelter, J. Chem. Phys. 124 (2006), 234104.
- [42] D. Wolf, P. Keblinski, S.R. Phillpot, J. Eggebrecht, J. Chem. Phys. 110 (1999) 8254.
- [43] E.E. Gdoutos, R. Agrawal, H.D. Espinosa, Int. J. Numer. Meth. Engng. 84 (2010) 1541.
- [44] S. Soliman, A. Elfalaky, G.H. Fecher, C. Felser, Phys. Rev. B 83 (2011), 085205.

- [45] K. Shinoda, K. Sugiyamat, K. Omote, Y. Waseda, *Int. J. Soc. Mater. Eng. Resour.* 4 (1996) 20.
- [46] Z. Somogyvári, E. Sváb, G. Mészáros, K. Krezhov, P. Konstantinov, T. Ungár, J. Gubicza, *Mater. Sci. Forum* 378–381 (2001) 701.
- [47] R. Hill, *Proc. Phys. Soc. A* 65 (1952) 349.
- [48] M. Jamal, S. Jalali Asadabadi, I. Ahmad, H.A. Rahnamaye Aliabad, *Comput. Mater. Sci.* 95 (2014) 592.
- [49] Z. Li, E.S. Fisher, J.Z. Liu, M.V. Nevitt, *J. Mater. Sci.* 26 (1991) 2621.
- [50] D. Fritsch, C. Ederer, *Phys. Rev. B* 86 (2012), 014406.
- [51] K. Dileep, B. Loukya, N. Pachauri, A. Gupta, R. Datta, *J. Appl. Phys.* 116 (2014) 103505.
- [52] O.L. Anderson, *J. Phys. Chem. Solids* 24 (1963) 909.
- [53] A. Roldan, D. Santos-Carballal, N.H. Leeuw, *J. Chem. Phys.* 138 (2013), 204712.
- [54] H. Guo, A.S. Barnard, *Phys. Rev. B* 83, 094112 (2011).
- [55] O.L. Anderson, H.H. Demarest Jr., *J. Geophys. Res.* 76 (1971) 1349.
- [56] H.M. Ledbetter, *Zeitschrift Für Naturforschung A* 31 (1976) 1539.
- [57] S. Mitra, editor, in: *Developments in Geochemistry*, Elsevier, 2004, pp. 673–709.
- [58] L.W. Finger, R.M. Hazen, A.M. Hofmeister, *Phys. Chem. Minerals* 13 (1986) 215.
- [59] S.B. Narang, K. Pubby, *J. Magn. Mater.* 519 (2021), 167163.
- [60] X.W. Zhou, H.N.G. Wadley, J.-S. Filhol, M.N. Neurock, *Phys. Rev. B* 69 (2004), 035402.
- [61] H. Perron, T. Mellier, C. Domain, J. Roques, E. Simoni, R. Drot, H. Catalette, *J. Phys.: Condens. Matter* 19 (2007), 346219.
- [62] A.T. Nelson, J.T. White, D.A. Andersson, J.A. Aguiar, K.J. McClellan, D.D. Byler, M. P. Short, C.R. Stanek, *J. Am. Ceram. Soc.* 97 (2014) 1559.
- [63] D. Levy, R. Giustetto, A. Hoser, *Phys. Chem. Minerals* 39 (2012) 169.
- [64] K. Shi, K. Zhou, L. Zhang, Z. Li, *J. Cent. South Univ.* 19 (2012) 2411.
- [65] L. Blaney, *Magnetite (Fe₃O₄): Properties, Synthesis, and Applications*, Volume 15 - 2007. Paper 5, 2007.
- [66] American Chemical Society (n.d.). <https://www.acs.org/content/acs/en/molecule-of-the-week/archive/m/magnetite.html>.
- [67] S.Z. Chavoshi, S. Xu, S. Goel, *Proc. Roy. Soc. A: Math., Phys. Eng. Sci.* 473 (2017) 20170084.
- [68] Y. Zhang, E.J. Maginn, *J. Chem. Phys.* 136 (2012), 144116.
- [69] S.L. Teich-McGoldrick, J.A. Greathouse, R.T. Cygan, *J. Phys. Chem. C* 116 (2012) 15099.
- [70] A.P. Thompson, S.J. Plimpton, W. Mattson, *J. Chem. Phys.* 131 (2009), 154107.
- [72] Soontrapa, Y. Chen, *Computational Materials Science* 50 (2011) 3271.